AD-A261 593

IGE

Form Approved
OMB No. 0704-0188

1a. REPORT SECURITY CLA	RESTRICTIVE MARKINGS
Unclassified	

2a. SECURITY CLASSIFICATION AUTHORITY	3. DISTRIBUTION / AVAILABILITY OF REPORT
MAR 2 1993	Approved for public release; distribution unlimited.
2b. DECLASSIFICATION / DOWNGRADING SCHEDULE	

4. PERFORMING ORGANIZATION REPORT NUMBER(S)	5. MONITORING ORGANIZATION REPORT NUMBER(S)
92-5	AFOSR-TR- 93 0004

6a. NAME OF PERFORMING ORGANIZATION	6b. OFFICE SYMBOL (If applicable)	7a. NAME OF MONITORING ORGANIZATION
New York University		Air Force Office of Scientific Research

6c. ADDRESS (City, State, and ZIP Code)	7b. ADDRESS (City, State, and ZIP Code)
Departments of Physics and Psychology 4 Washington Place New York, NY 10003	Building 410 Bolling AFB, DC 20332-6558

8a. NAME OF FUNDING / SPONSORING ORGANIZATION	8b. OFFICE SYMBOL (If applicable)	9. PROCUREMENT INSTRUMENT IDENTIFICATION NUMBER
AFOSR	NL	AFOSR-90-0221

8c. ADDRESS (City, State, and ZIP Code)	10. SOURCE OF FUNDING NUMBERS			
Building 410 Bolling AFB, DC 20332-6558	PROGRAM ELEMENT NO.	PROJECT NO.	TASK NO	WORK UNIT ACCESSION NO.
	61102F	2313	BS	

11. TITLE (Include Security Classification)
Imaging Regional Changes in the Spontaneous Activity of the Brain: An Extension of the Minimum-Norm Least-Squares Estimate

12. PERSONAL AUTHOR(S)
J-Z. Wang, L. Kaufman, and S.J. Williamson

13a. TYPE OF REPORT	13b. TIME COVERED	14. DATE OF REPORT (Year, Month, Day)	15. PAGE COUNT
Manuscript	FROM 920201 TO 930214	930120	16

16. SUPPLEMENTARY NOTATION

17. COSATI CODES			18. SUBJECT TERMS (Continue on reverse if necessary and identify by block number)
FIELD	GROUP	SUB-GROUP	Magnetic source imaging, MSI, alpha rhythm, magnetic inverse problem, spontaneous brain activity

19. ABSTRACT (Continue on reverse if necessary and identify by block number)

A method has been developed to determine the distribution of average spontaneous neuronal activity across the cerebral cortex from measurements of the field pattern across the human scalp. Computations of the mean short-term power, as well as the covariance between pairs of sensors, provide sufficient information to obtain a best estimate for the distribution of mean short-term image current power, as well as the covariance of image current between different locations on cerebral cortex. This method has applications for determining the spatial locations of alpha power suppression as regions of cortex participate in sensory or cognitive functions.

93-04302

20. DISTRIBUTION / AVAILABILITY OF ABSTRACT	21. ABSTRACT SECURITY CLASSIFICATION
☐ UNCLASSIFIED/UNLIMITED ☒ SAME AS RPT ☐ DTIC USERS	Unclassified

22a. NAME OF RESPONSIBLE INDIVIDUAL	22b. TELEPHONE (Include Area Code)	22c. OFFICE SYMBOL
Dr. John F. Tangney	202-767-5021	NL

DD Form 1473, JUN 86 *Previous editions are obsolete.* SECURITY CLASSIFICATION OF THIS PAGE

UNCLASSIFIED

99

Imaging regional changes in the spontaneous activity of the brain: an extension of the minimum-norm least-squares estimate *

Jia-Zhu Wang, Lloyd Kaufman and Samuel J. Williamson

Neuromagnetism Laboratory, Departments of Physics and Psychology, and Center for Neural Science, New York University, New York, NY 10003 (USA)

Summary   This paper describes methods for inferring mathematically unique local distributions of primary cortical current that underly changes in the average pattern of power of the ongoing ("spontaneous") extracranial magnetic field of the brain. In previous work we demonstrated that mathematically unique solutions to the inverse problem are possible for current sources of the brain's field, without assuming a small set of current dipoles as a source model. In principle, it is possible to locate and delineate patterns of current of any configuration. In practice this approach applies to synchronized neuronal activity, e.g., activity which is known to underly average evoked or event-related brain responses. This paper extends that approach to local changes in incoherent activity, e.g., activity yielding fields or potentials that tend to be self-canceling when averaged over time. This includes the spontaneous brain activity normally treated as background noise when it accompanies event-related responses. We demonstrate that local changes in this ongoing incoherent activity may also be uniquely delineated in space and time. The solution is a covariance matrix characterizing activity across an image surface. Its diagonal elements represent the spatial pattern of mean current power. Evidence is reviewed indicating that the distribution of the brain's magnetic field, due to *both* its synchronized and incoherent neural activity, is affected by early sensory-perceptual processes and by higher cognitive processes. Hence, in principle, the ability to delineate both kinds of sources in space and time makes it possible to form more comprehensive dynamic functional images of the human brain.

Key words: Inverse solution; Minimum-norm least-squares inverse; Neuromagnetic measurements; Magnetic source image

Recent theoretical developments make it possible in principle to locate and delineate the pattern of electrical activity of the cortex underlying event-related changes in the brain's magnetic field. Given prior knowledge of the underlying geometry of the cortex, solutions to this problem of source identification can be mathematically unique, despite the widely held assumption that such solutions must inevitably be ambiguous. As a practical matter, these mathematically unique solutions to the inverse problems are relevant to sources of stable field patterns, i.e., those that can be recovered from background noise by means of signal averaging. Thus, they apply to fields of evoked or event-related responses. The spatial distribution of fields due to the intrinsic activity of the brain, i.e., those that accompany the event-related fields, change with time, and are therefore considered to be incoherent. Owing to this spatio-temporal incoherence, they tend to be self-canceling when averaged. This self-cancellation permits the event-related response to emerge during averaging. However, recent experimental work demonstrated that, despite its incoherence, the level of the intrinsic activity of the brain changes as subjects perform different mental tasks. Further, these task-relevant changes arise from circumscribed regions of the brain, and the regions involved vary depending upon the nature of the task.

Although complicated and incoherent, the specific spatial distribution of the extracranial spontaneous field is strongly dependent upon the underlying geometry of the cortex as well as the relative amounts of activity across its surface. However, when the variance (power) of the spontaneous extracranial field is measured to yield a spatial map of average field power, stable spatial patterns may emerge. These patterns are known to be dependent upon both the underlying geometry and the relative amounts of activity across the cortical surface. In this paper we demonstrate for the first time that mathematically unique solutions to the inverse problem also exist for source configurations that underly the external distribution of field power. The solution to this problem also requires prior knowledge of the geometry of the cortical surface. However, mathematically the proof is quite different from the one establishing that sources of event-related fields may

also be identified. Solutions to the inverse problem for event-related field sources and for differential levels of intrinsic brain activity provide complementary information. Together they are capable of providing a more complete picture of brain activity than can be obtained from either type of activity alone. We now provide a detailed and documented account of these concepts.

Ionic currents flowing within the brain's neurons are accompanied by superimposable magnetic fields that encircle entire populations of concurrently active neurons. Where the coherent (synchronized) activity of the neurons is limited in area — so that the extent of cortex involved is small relative to the distance at which its field is measured — the external field is essentially indistinguishable from one produced by a current dipole. Field measurements make it possible to determine the 3-dimensional location, orientation and strength of this equivalent current dipole (Cuffin and Cohen 1977; Williamson and Kaufman 1981, 1987). Typically, a statistical method is used to fit the observed field pattern to one that would be produced by a hypothetical underlying current dipole. However, a dipolar source deduced from an observed field is but one of many possible solutions to the so-called *inverse problem* which, in general, has no unique solution. Many different source configurations could produce virtually the same dipolar field pattern.

Generally, the inherent ambiguity of inverse solutions makes it impossible to be certain of the actual generator of an observed field pattern, as the field may be due to the activity of an assemblage of dipoles distributed throughout the intracranial space. In fact, Scherg and Von Cramon (1985) and Scherg (1990) devised a spatio-temporal method in which best fits to a multiple dipole source is sought. Mosher et al. (1992) demonstrated that the linear moment parameters can be separated from the non-linear location parameters using similar approaches. However, it is not necessary to restrict solutions to those predicated on specific source models, e.g., dipoles. For example, in recent work on magnetic source imaging it was assumed that the current to be imaged flowed parallel to a plane or to each of several parallel planes, but no particular configuration was assumed. In some of these studies (Dallas 1985; Kullmann and Dallas 1987) the shape of an arbitrary planar current distribution producing an observed external field was computed from the inverse of the Fourier transform of the field. However, this approach does not provide a unique solution to the inverse problem, as magnetic field measurements alone do not contain enough information to assure uniqueness. Nevertheless, within constraints due to limited bandwidth of the spatial frequency content of the field (because of the distance between the source and the sensor), and errors due to additive noise, the method does yield a current distribution in any arbitrarily se-

lected plane or subspace within a volume. What is lacking is unambiguous knowledge of the space actually occupied by the primary current distribution within the volume. Other authors describe similar approaches (Dallas et al. 1987; Kullmann and Dallas 1987; Singh et al. 1984; Roth et al. 1989; Tan et al. 1990).

Another related approach is that of Hämäläinen and Ilmoniemi (1984, 1991), Kullmann et al. (1989), Okada and Huang (1990), and Graumann (1991), who used linear estimation methods to determine the current distributions from their field patterns. We should also note the recent work of George et al. (1991), Greenblatt (1991), Okada et al. (1991), Robinson (1991), Szinger and Kuc (1991), etc. who employed related methods to form magnetic source images. Kullmann (1991), summarizing much of the work based on this approach, describes how the linear estimation method (within the bounds of precision due to noise and spatial filtering of the observed field) reveals recognizable images of the distributions when they are projected onto an arbitrary plane within the conducting volume. However, if the surfaces onto which the solutions are projected are truly arbitrary, then the resulting inverse solution is not unique. Similar problems are associated with probabilistic approaches described by Clarke et al. (1989), and by Ioannides et al. (1989, 1990), although in principle they too can deal with current configurations on a plane or stacks of planes within a conducting volume.

It is obvious that the actual surface occupied by the primary current configuration is knowable. In fact, the major sources contributing to the magnetoencephalogram are known to exist in the cerebral cortex. Furthermore, ample electrophysiological evidence supports the assumption that the primary current flow is, on average, normal to the surface and not parallel to it (George et al. 1991; Kaufman et al. 1991; Wang et al. 1992). This *a priori* information is one vital ingredient of methods for finding mathematically unique solutions to the inverse problem.

The geometry of the surface containing the primary sources needed to achieve a mathematically unique solution to the inverse problem may be obtained from high-resolution MRI scans. Moreover, basic electrophysiology teaches us that postsynaptic potentials leading to axial intracellular current flow, e.g., in pyramidal cells within cortical macrocolumns, is predominantly normal to the surface of the cortex. These axial (primary) currents make the major contribution to the field measured normal to the surface of the scalp. Thus, according to Wang et al. (1992), any arbitrary pattern of current would consist of elements of current flowing in the same direction normal to the surface of some region of cortex. The problem is thus constrained to discovering the net strength of this current flow and the area of cortex it occupies.

The linear estimation method of Hämäläinen and Ilmoniemi (1984, 1991) and Crowley et al. (1989) employs a so-called *minimum-norm* criterion, which refers to the fact that the accepted solution is one in which the net squared current (the square of the current integrated over the surface) predicting the observed field is a minimum, as compared with the net squared current of all possible candidate source configurations. It should be noted that Hämäläinen and Ilmoniemi (1984) may have been the first to recognize the importance of prior knowledge of the underlying source geometry. However, even when supplemented with prior knowledge of the source surface, the minimum-norm criterion they and others have employed is still insufficient to produce a solution that qualifies as mathematically unique. Wang et al. (1992) recognized that the minimization of the sum of the squares of the differences between the observed or measured field pattern external to the scalp and a theoretical pattern computed from the source configuration meeting the minimum-norm criterion leads to a unique solution. This minimum-norm least-squares (MNLS) criterion falls naturally out of the specific type of the generalized inverse Wang et al. adopted for this problem (Penrose 1955). The earlier investigators who adopted this same generalized inverse did not seem to recognize its least-squares feature and that it makes a unique solution possible.

MNLS solution for coherent sources

Review of basic concepts

The MNLS approach can be simply explained by considering a geometry illustrated in Fig. 1 which shows a *source surface* composed of two planar surfaces at right angles to each other, and an *observation surface* above and at right angles to the source surface. Since the source surface is presumed to be known, it coincides with the *image surface* on which the inferred current pattern, flowing normal to it, is to be located. Fig. 2 illustrates a field pattern on the observation surface generated by single dipole on the source surface. The image of the source computed from the field is shown on the image surface. Fig. 3 shows a region of one plane of the source surface containing a crescent-shaped pattern of current elements. These currents are all flowing in the same directions at once. Thus, we say that they are coherent or synchronized. The plots in the middle panels of Fig. 3 show the inverse solutions across the image surface. The inverse solution clearly resembles the original source. Wang et al. (1992) provide several examples of this type of result, thus providing demonstrations of unique inverse solutions given the conditions specified above.

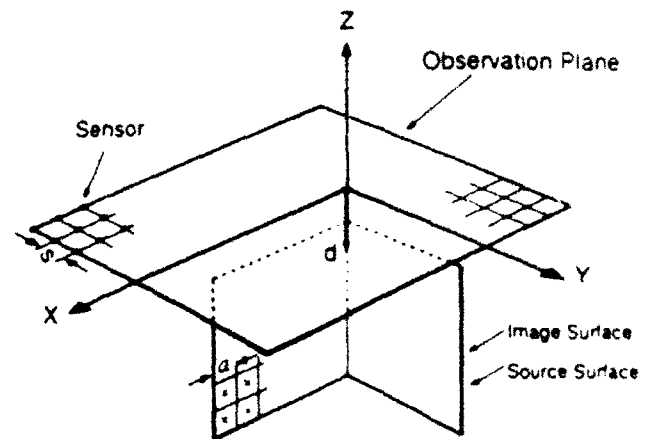Thus far we have said little about the actual meas-

Fig. 1. Model configuration in which the component of the magnetic field B_i normal to the *observation plane* is measured by "point sensors" at the nodes of a grid composed of cells of size s. The center of the observation plane lies at $x = +2$ cm. The *source space* is an L-shaped surface formed by two vertical walls. The top edges of the walls are 1 cm below the observation plane and the corner joining the walls coincides with the z-axis. The *image surface* coincides with the source surface and inverse computations are carried out to deduce the source density on a grid of size a.

urements made on the observation surface. At every position where a measurement of the field is made, the actual measure depends upon the contribution of each current element of the source, which in turn is dependent upon the strength of the element, its orientation relative to the sensing coil, and its distance from the coil. Further, it depends upon the geometry of the coil itself and the orientation of the coil with respect to the
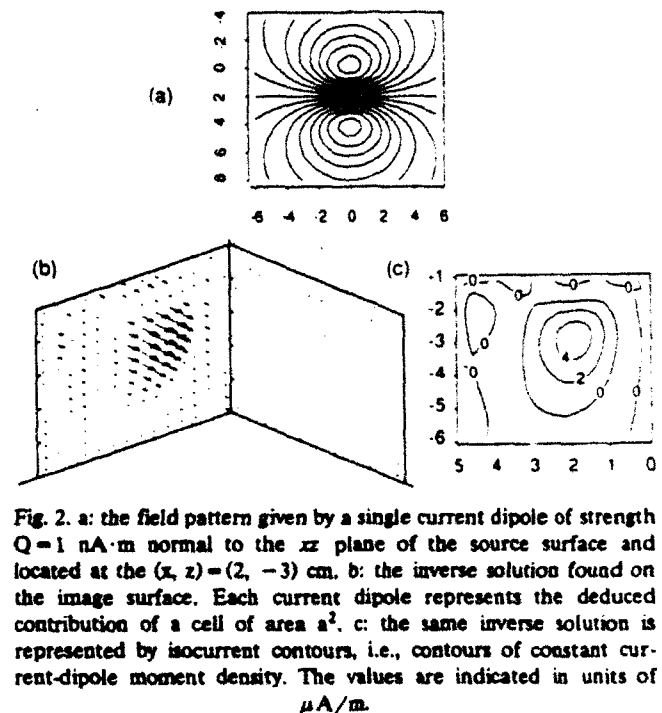

Fig. 2. a: the field pattern given by a single current dipole of strength $Q = 1$ nA·m normal to the xz plane of the source surface and located at the $(x, z) = (2, -3)$ cm. b: the inverse solution found on the image surface. Each current dipole represents the deduced contribution of a cell of area a^2. c: the same inverse solution is represented by isocurrent contours, i.e., contours of constant current-dipole moment density. The values are indicated in units of $\mu A/m$.

observation surface. The effects of all of these factors may be taken into account through the concept of coil's lead field (see below). Points on the image surface are taken to represent elements of a current configuration that would produce the values of $\vec{B}_i$ measured at positions $\vec{r}_i$, $i = 1,..., m$, on the observation surface, where the measures are weighted by the sensitivity of the respective detection coil at the various positions. The distribution of the current across the cortex can be represented as an array of closely spaced current dipoles of suitable strength Q_j at the positions $\vec{r}_j'$ on the source surface, the values of $\vec{Q}_j$, where $j = 1,..., n$ determine the observed field pattern. The matrix relating the values $\vec{B}_i$ at $\vec{r}_i$ to a current dipole of unit strength ($|Q_j| = 1$ A·m) at $\vec{r}'$ is referred to as the lead field matrix L. A more technical account of the lead field concept and that of the minimum-norm least-squares (MNLS) approach follows. The non-mathematical reader may skip the equations in the sections with a leading asterisk, but much of the text is understandable without them.

Lead field analysis. In common with all of the other linear estimation and related methods, the approach of Wang et al. (1992) assumes that the primary current underlying the observed field is intracellular and that the secondary (volume) currents make a negligible contribution. Further, the primary current is assumed to be distributed within a finite space Ω. The

law of Biot and Savart relates the magnetic induction $\vec{B}(\vec{r})$ to the current density $\vec{J}(\vec{r}')$ within Ω

$$\vec{B}(\vec{r}) = \frac{\mu_0}{4\pi} \int_\Omega \frac{\vec{J}(\vec{r}') \times (\vec{r} - \vec{r}')}{|\vec{r} - \vec{r}'|^3} dr'^3 \qquad (1)$$

In reality, the number of observations of magnetic field is finite. While the brain anatomy is complicated, as pointed out earlier, in principle, it has a known geometrical configuration Ω. It follows that the observations of the normal components of field B_i are linearly related to the current source density by

$$B_i = \int_\Omega \vec{L}_i(\vec{r}') \cdot \vec{J}(\vec{r}') \, dr'^3, \quad i = 1,...,m. \qquad (2)$$

where $\vec{r}'$ is the position vector within the source region Ω, ($\vec{r}' \in \Omega$). The vector form $\vec{L}_i(\vec{r}')$ is known as the lead field (Plonsey 1972; Williamson and Kaufman 1981). The lead field $\vec{L}_i(\vec{r}')$ accounts for the sensitivity to the magnetic flux of the ith pickup coil at position $\vec{r}_i$ produced by unit source current density at $\vec{r}'$. The lead field within Ω is determined by the geometry and orientation of the detection coil. For the present we make the simplifying assumption that the detection coil is so small that it may be considered to be a point.

To prove the principles presented here, it is not necessary to employ the actual convoluted cerebral cortex as a source surface. Instead, in the interest of clarity, we employ as a source space Ω a simple folded
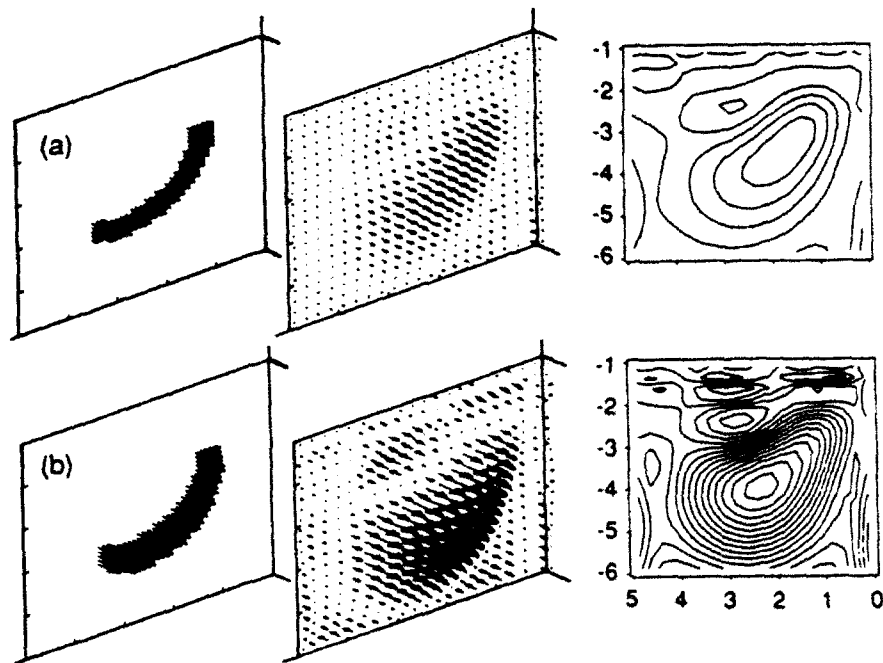

Fig. 3. a: an extended crescent-shaped source of uniform current-dipole density on the source surface with upper edge at $z = -2.5$ cm and lower at -4.5 cm. The inverse solution on the image surface is shown on the right as a distribution of current dipoles and as isocontours for current-dipole moment density. The solution has a similar crescent-shaped outline, but is weakened and somewhat spread at greater depths. b: the same source, but the current density at the bottom is 4 times that at the top. In this case a field sampling interval of $s = 0.5$ cm was used and measurements were made across a 14 cm × 14 cm observation plane.

surface layer of uniform thickness w. Therefore, the volume integral is reduced to a surface integral. If we further divide the surface into a grid of n cells with area $\Delta S_j'$, centered at position $\vec{r}_j'$ and assume that current density is constant within each small area, we can replace the integral of Eq. 2 with a summation sign. Eq. 2 becomes

$$B_i = \sum_{j=1}^{n} \vec{L}_i(\vec{r}_j') \cdot \vec{J}(\vec{r}_j') w \Delta S_j', \quad i = 1,\ldots,m. \tag{3}$$

Note that $\vec{J}(\vec{r}_j') w \Delta S_j'$ bears the dimension of current dipole: ampere-meter. In matrix representation Eq. 3 can be written as

$$B = LQ, \tag{4}$$

where b and Q are column vectors and L is a $m \times n$ matrix.

As stated earlier, it is well known that the inverse solution of Eq. 4 is not unique. Mathematically, this is because there may exist a family of solutions Q^* of the following homogeneous equation corresponding to Eq. 4

$$LQ^* = 0. \tag{5}$$

We know that the solutions of Eq. 5 may have an infinite number of elements. If $\hat{Q}$ is an estimated source of Eq. 4 then any combination of $\hat{Q} + Q^*$ could be the solution of Eq. 4. The component Q^* represents the "magnetically silent" sources, which produce no magnetic field on the observation plane.

The unique minimum-norm least-squares inverse of the field. Despite the obstacle posed by the non-uniqueness of inverse solutions, we claim that the source can be estimated by minimizing the square of the residual error between the measurements and theoretical computations from the estimated sources. In the presence of noise, we minimize the weighted least-squares error (or the χ^2 statistic)

$$\text{minimum of } \sum_{i=1}^{m} \left(\frac{\hat{B}_i - B_i}{\sigma_i} \right)^2 \tag{6}$$

where $\hat{B}_i$ represents values of the field computed from the estimated source, B_i the measured values of the field, and σ_i the rms noise. The corresponding matrix expression of Eq. 6 is

$$\text{minimum of } \|L'\hat{Q} - b'\|^2. \tag{7}$$

where $\| \ \|$ is the Euclidean norm of a vector, L' the weighted matrix with element Lij/σ_i, and b' the weighted vector with element B_i/σ_i in the presence of noise. In what follows we will drop the prime in L and b for simplicity. However, it is understood that they refer to the weighted matrix and vector whenever noise is present.

In statistics one generally deals with cases where the number of measurements, and therefore the number of equations, is greater than number of unknowns ($m > n$),

and the unknowns are always linearly independent. It is only in such conditions that the least-squares fit will give a unique estimate.

In reality the number of unknowns may exceed the number of equations. Also, the n unknowns may not all be linearly independent of each other because of noise or an accumulation of round-off errors. In this case the least-squares criterion will not lead to a unique estimate. That is to say, there may exist a set of solutions which all fulfill the least-squares criterion. If we further select one solution from such a set and require that the square of the image current ("power") integrated over the image surface also be a minimum, the resulting estimate has the least residual error and has itself the minimum power amongst all least-squares solutions

$$\text{minimum of } \|\hat{Q}\|^2 = \text{Minimum of } \sum_{j}^{n} \hat{Q}_j^2 \tag{8}$$

Equivalently, we seek the solution that minimizes the following Euclidean norm of the vector Q

$$\text{minimum of } \|\hat{Q}\| = \text{Minimum of } \left(\sum_{j}^{n} \hat{Q}_j^2 \right)^{1/2}. \tag{9}$$

The above equation is the so-called *minimum-norm* which, as we pointed out earlier, together with Eq. 6 (or 7) represent both the least-square residual error and the minimum power of the inverse solution.

There exist many different types of generalized inverses in mathematics. This particular type which has the feature of the least residual error of the measurements and the minimum power of the source is known as the Moore-Penrose inverse, or pseudo-inverse (Ben-Israel and Greville 1974; Barnett 1990). We have adopted the terminology of minimum-norm least-squares (MNLS) inverse because the name implies its properties. More importantly, the MNLS inverse is proven to be mathematically unique.

The unique MNLS inverse estimate of Eq. 4 is given by

$$\hat{Q} = L^+ b, \tag{10}$$

where L^+ is the MNLS inverse matrix of L. The structure of L^+ and how to compute it are discussed in detail in Wang et al. (1992). Here we mention only that the method of singular value decomposition (SVD) is used in computing L^+ (Press et al. 1986; Ciarlet 1991). Nevertheless, we list a few properties of the MNLS inverse which could be useful to the reader in actual computations (Ben-Israel and Greville 1974; Ciarlet 1991).

$$(L^T)^+ = (L^+)^T \tag{11a}$$

$$L^+ = (L^T L)^+ L^T \tag{11b}$$

$$L^+ = L^T (L L^T)^+ \tag{11c}$$

MNLS solution for incoherent sources

Incoherent versus coherent distributed sources

It is important to emphasize that the MNLS method discussed thus far applies only to coherent (synchronous) patterns of primary current and, as recounted above, many authors have dealt with various facets of the problem. Synchronized current elements, where current flows normal to the surface of the cortex, provide a reasonable source model for spatially coherent event-related fields (Kaufman et al. 1991a). Time averages are dominated by the spatially coherent fields, while those of the incoherent background activity tend to be self-canceling. Evoked fields are stable in space, while the spatial distributions of the fields of the incoherent background activity change with time. However, if the fields due to ongoing incoherent activity are squared to obtain *field power*, and the resulting spatial patterns of power are averaged, then the configuration of the averaged power pattern is determined by the underlying geometry of the source surface, as well as by the statistics of the elements of current of which its source is composed (Kaufman et al. 1991a). Also, if, on average, a region of the source surface exhibits either more or less asynchronous activity than its surroundings, the average field power pattern is affected and is related to the location and shape of the region in question. This suggests that it is possible to locate and delineate differentially active regions of cortex, even when that activity is incoherent. In fact, simple methods previously applied to dipole localization (Williamson and Kaufman 1981) were successfully extended to apply to the localization of the center-of-gravity of a region of incoherent activity that was either stronger or weaker than that of its incoherently active surroundings (Kaufman et al. 1991a).

Many experiments now show that incoherent activity revealed by power patterns of extracranial fields are differentially affected by the performance of cognitive tasks. Such differential effects are localized to different regions of the scalp, depending on the nature of the cognitive task. These experiments motivated the present theoretical study. For example, Kaufman et al. (1991b) demonstrated that power of the spontaneous alpha activity originating in the right temporal lobe is suppressed while subjects scan memory for previously heard musical tones. The duration of this suppression increases linearly with the size of the memory set, as does reaction time when performance is relatively free of errors (Sternberg 1966). Further, while suppression is detected elsewhere, its duration is not related to the time required to scan memory. The interhemispheric differences among these effects are far more profound than those encountered in event-related potential studies (Regan 1989). The N100 component evoked by the same tones and detected electrically at Cz does not

covary systematically with RT. Further, the magnetic counterpart to N100 does not vary consistently with set size either, and changes in its amplitude with set size differ dramatically across the hemispheres. N100 is due to the activity of neurons synchronized by the stimulating event and may well reflect different attentional strategies, but it does not reflect operations on short-term memory. Similarly, Kaufman et al. (1991b) reviewed an extensive P300 literature on this subject and found that neither the latency nor the amplitude of P300 (which is also due to coherent activity of neurons) varies linearly with set size. Further, sometimes there is no change at all in P300 with set size, although the RTs of the same subjects increase with set size.

Kaufman et al. (1990) also found suppression of alpha frequencies when subjects scanned memory for visual forms. However, in this case the effect was measured over the visual areas. This result was recently confirmed by Cycowicz et al. (1992). Also, when subjects engage in verbal tasks in response to visually presented words, the suppression related to performing the task is not present over the visual areas (Kaufman et al. 1989), but it is over the left frontotemporal areas (Cycowicz et al. 1992).

Pfurtscheller et al. (1977, 1988a,b) observed dramatic changes in alpha power in the EEG over different cortical regions, depending upon the nature of the task. These effects were often bilateral and difficult to localize from the EEG data. However, the reference-free MEG clearly establishes that these suppression effects are local, and not merely due to generalized arousal.

All of this serves to motivate the present paper. It is clear that early sensory-perceptual and some cognitive processes are reflected in the coherent event-related responses. It is equally clear that local changes in incoherent activity reflect other cognitive processes and may even be related to perceptual processes as well. The two measures complement each other, and neither alone is an adequate basis for building a cognitive neuroscience. The MNLS method has now made it possible to delineate the cortical areas involved in the coherent aspect of brain activity. To complete the picture we now extend the MNLS method to make it possible to find unique inverse solutions to the problem of delineating the cortical areas exhibiting changes in incoherent activity.

The minimum-norm least-squares inverse of power. The basic problem attendant upon identifying differential incoherently active regions is that we deal with average field power as the basic measure and not field *per se*. We introduce a novel mathematical development for solving the inverse problem for such measures.

Previously the values of the field B_i measured normal to the observation surface at m positions were

used to form a column vector **b** of m elements. If we now introduce an auto-correlation matrix $\mathbf{B}_p$ in terms of the vector **b**, we obtain

$$\mathbf{B}_p = \mathbf{b}\mathbf{b}^T, \tag{12}$$

with elements $(\mathbf{B}_p)_{ij} = B_i \cdot B_j$, where $i, j = 1, 2,..., m$. Therefore, the diagonal elements of $\mathbf{B}_p$ are the field power B_i^2, rather than field.

Manipulations of Eq. 4 reveal a new linear model which relates field power to the source power, as opposed to a linear relation between field *per se* and source strength as given by Eq. 4. Thus,

$$\mathbf{B}_p = \mathbf{L}\mathbf{Q}_p\mathbf{L}^T. \tag{13}$$

where $\mathbf{Q}_p$ is the auto-correlation matrix of source image, $(\mathbf{Q}_p)_{kl} = Q_k \cdot Q_l$, $k, l = 1, 2,..., n$, with the diagonals as the power of the source. Note the difference between Eq. 4, which has a matrix and two vectors, and Eq. 13, which contains all matrices. Fortunately, for the matrix equation Eq. 13 there also exists a unique MNLS inverse. With the help of the MNLS inverse theory (Penrose 1955; Ben-Israel and Greville 1974) and the property given in Eq. 11a, we are able to derive the MNLS inverse of the source power for a given field power distribution

$$\hat{\mathbf{Q}}_p = \mathbf{L}^+ \mathbf{B}_p (\mathbf{L}^+)^T \tag{14}$$

Applying this equation makes it possible to delineate regions of cortex whose levels of incoherent activity deviate from a baseline because of some ongoing cognitive process, or even because of effects of transient ischemia, cortical hyperactivity, abnormally low metabolic level, etc.

If we use $<\ >$ to denote the time average, and take the time average of the field power given by Eq. 14, we obtain

$$\langle \hat{\mathbf{Q}}_p \rangle = \mathbf{L}^+ \langle \hat{\mathbf{B}}_p \rangle (\mathbf{L}^+)^T. \tag{15}$$

Note that, the lead field matrix **L** is time invariant, and so is its MNLS matrix $\mathbf{L}^+$, provided that the measures made at different times are made at the same positions. This is the basis for the extended MNLS inverse.

It is important to note that the concept of direction of current flow is totally meaningless when dealing with field power related to such phenomena. These differ from evoked responses and similar time-evoked events where direction of underlying current flow is of considerable importance.

Methods and results

Image representation
An inverse solution for a set of field measurements can be represented in two convenient ways. One is by

an array of current dipoles oriented perpendicular to the image surface, each dipole placed at the center of a cell of area a^2. The image is thus represented by the distribution of strengths of the dipoles, each representing the current dipole moment per cell (as shown in Fig. 2b). Another representation is the pattern of isocontours on the image surface that describe the dipole moment density (as shown in Fig. 2c). Both of these are sometimes referred to as the "current image" obtained from the data.

An inverse solution for a set of time-averaged field power measurements can be represented in analogous ways. Instead of an array of current dipoles across the image surface whose moments are specified, we use an array whose time-averaged square moments are specified (as shown in Fig. 6b). Arrows directed toward the viewer indicate positive strength for the inverse solution. Also, the image can be specified by the pattern of isocontours that describe the mean square moment density. Both of these can be referred to as the "current power image."

Simulations
The results of this theoretical work are in the form of simulations in which surfaces representing the cerebral cortex (or any other thin layer of spontaneously active neural tissue within the brain) are populated by a large number of perpendicular primary current elements (dipoles) of random orientation and magnitudes. Subsets of these elements are either incremented or decremented in magnitude, and the net fields of all of the elements are summed at the observation surface (Fig. 1). It is to be noted that the simulations described here are merely illustrations of how the extended MNLS method may be employed, and are not of themselves proof of the uniqueness of the solution. The uniqueness is inherent in the mathematics of the MNLS inverse.

In the simulation, the current dipole moments populating the source surface are sampled from a uniform distribution, and a new random seed is applied to the random number generator prior to the selection of any array. This assures an ever-changing field pattern at the observation surface. The field at each detector is squared to obtain field power (Eq. 12). One hundred such plots representing different time series are averaged together to form the average power plot. Then the extended MNLS method is applied to deduce the image of the source. This image is compared with the configuration of the original source to determine whether the inverse solution is a reasonable estimate of the actual source which, in this case, is either the incremented or decremented region of incoherent activity.

In the various simulations carried out here, the background activity is spread over the entire source

surface (the L-shaped wall of Fig. 1). Each wall of the surface is assumed to be 5 cm × 5 cm. The randomized magnitudes and directions of current flow (to simulate background "noise") are given values that range from $-1 \rightarrow +1$. It is important to note that there is one major difference between the walls of our source model and the actual cortex. The contours of the latter are rounded and not sharply terminated. Rounded contours of the actual cortex insure a gradual rotation of its macrocolumns, with those in a sulcus being largely tangential in orientation with respect to the surface, and those approaching a gyrus tending to become more nearly radial in orientation. Since the latter produce much weaker fields at the surface than do the tangential current elements within the wall of a sulcus, there is a graduated fall-off of the contributions of elements nearer the skull. To simulate this in our model we allow a smooth attenuation of the magnitudes of the still randomly selected dipoles beginning about 0.5 cm away from the top and side edges of the L-shaped wall and reaching zeros at the edge.

As indicated above, using different initial random seeds, 100 samples of source configurations were generated. The bottom of Fig. 4 is one of the samples. Field values are computed for each sensor on the 12 cm × 12 cm observation plane, which is 1 cm above the top edge of the source surface. In this simulation the sensors are spaced about 1 cm apart. As indicated, the 100 plots of field power thus generated are averaged.
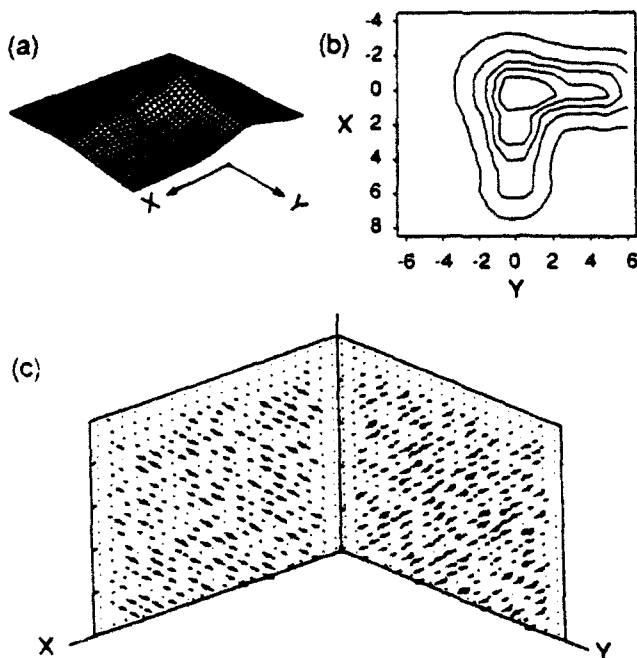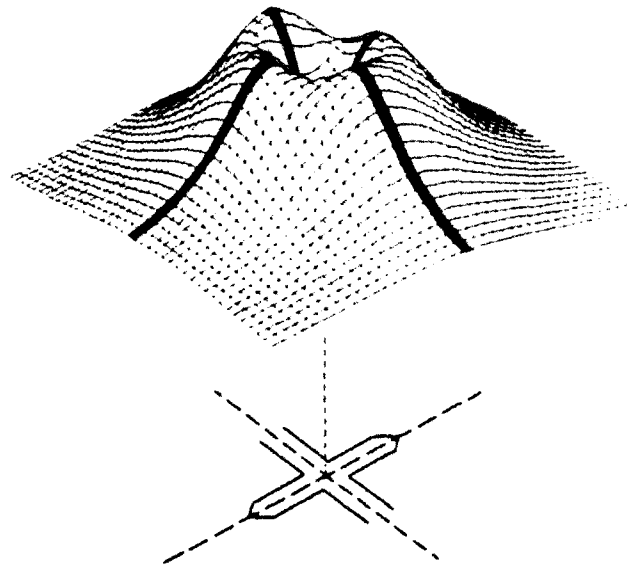

Fig. 5. Simulation for average field power computed in the same manner as for that of Fig. 4, except that the underlying source surface was of a more complicated shape. The cross-like shape shown below is the outline of fissures 4 mm wide separating "cortical" walls about 2 cm long and 2 cm wide and extending about 3 cm into a model "head" (Kaufman et al. 1991a).

This is illustrated by the 3-D power plot in Fig. 4a. It is of some interest to compare this plot with one of those depicted in Kaufman et al. (1991a) shown here as Fig. 5, where the underlying cortex was simulated by a cross-shaped arrangement of sulci. There was clearly a 4-lobed power pattern which was topologically related to the shape of the underlying structure. In this case the average power pattern resembles the shape of the underlying L-shaped structure — once again demonstrating the dependency of average field power on structure. It is worth noting in passing that this confirms our earlier conclusion that the actual geometry of the cortex must be explicitly taken into account if one is to understand scalp-detected phenomena, whether they be potentials or fields. In any event, in this case the average field power plot reveals the existence of the underlying L-shaped source surface when the incoherent background activity is uniform on average over time. As we shall see below, departures from uniformity also affect the shape of the pattern.

Fig. 4. a: average field power across the observation plane from a random array of dipoles with strengths ranging from -1 to +1 computed for 100 such independent random samples, one of which is illustrated in (b). c: contour plot of the average field power, whose two extensions lie over the walls of the source space.

Incremented incoherent activity

As a first test of the method, on average, the current dipole moment (amplitude) of a small circular region of radius 0.6 cm on one wall is enhanced by a factor of 10 as compared with the otherwise uniformly distributed activity of its surroundings, which is as described above. Fig. 6a shows one sample of 100 such source distributions. Note that the arrows signify current elements where the directions of current flow are randomly related to each other, unlike the sources of
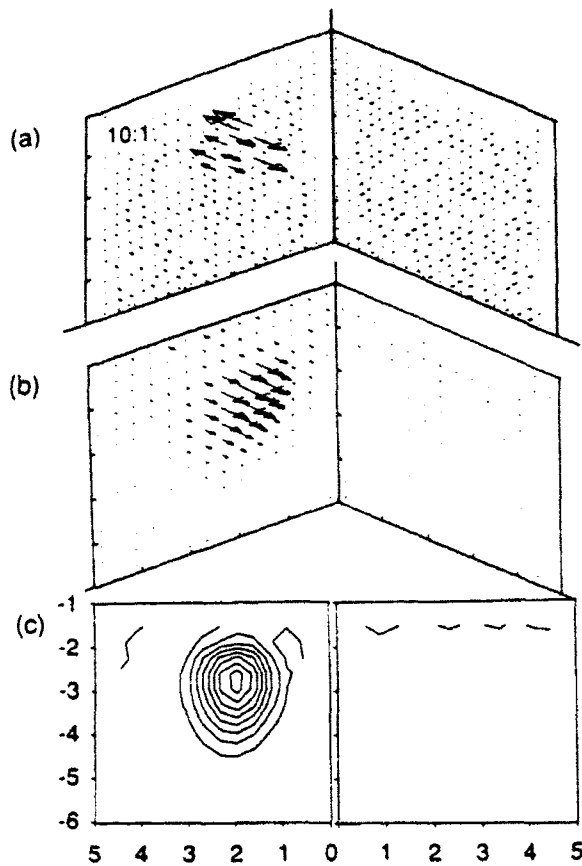
tours are centered on a point at the coordinates (x, z) = (2, −3) cm, which was the exact center of the original incremented current distribution of the source surface.

We next consider the case of two incremented circular regions, located on the source surface at the coordinates (x, z) = (2, −3) cm, and (y, z) = (2, −3) cm. While the current elements vary at random over time inside as well as outside the incremented regions, the ratio of averaged amplitude of the two incremented regions relative to their surroundings is 10:1. One of the 100 source samples is shown in Fig. 7b. Fig. 7a is the plot of the field power averaged over all 100 samples. It is of some interest to compare this plot with the L-shaped plot of Fig. 4, which is based on an average of 100 samples of randomly selected current elements where there is no net increment or decrement of any region. When two regions are, on average, more "active" than their surrounding, the L-shaped plot is transformed into one with three lobes, thus illustrating how both the geometry of the source surface and the statistics of its activity affect the distribu-

Fig. 6. a: the source surface of Fig. 1 is populated with a large number of current dipoles of randomly selected orientations and strengths, but those within a small (0.6 cm radius) region are, on average, 10 times stronger than those in the surrounding. The current power image distribution (b) and isopower density contours (c) are shown on the image surface. The arrow length in (b) is proportional to the average power at each location.

evoked responses. We first computed the average field power distribution at the sensors on the observation surface and the correlations among different sensors (Eq. 12). Then, in a one-step process, we computed the extended MNLS inverse over the entire image surface. According to Eq. 15, if the time average of field power is used, rather than field, the resulting inverse solution gives the time-averaged current power image.

Since the extended MNLS approach guarantees that the result is the best (in the sense of the least-square residual error between the measurements and the estimated field values) an iterative search process in which residual errors are compared at each step to find a minimum is unnecessary (as in a typical non-linear least-squares method). Fig. 6b is a perspective view of the current power image derived from the extended MNLS inverse. The power at each location is indicated by the length of an arrow, whose direction is arbitrarily chosen to be toward the reader. Heads are included to better illustrate their length. Fig. 6c is an isocontour plot representing the same inverse. Note that the con-
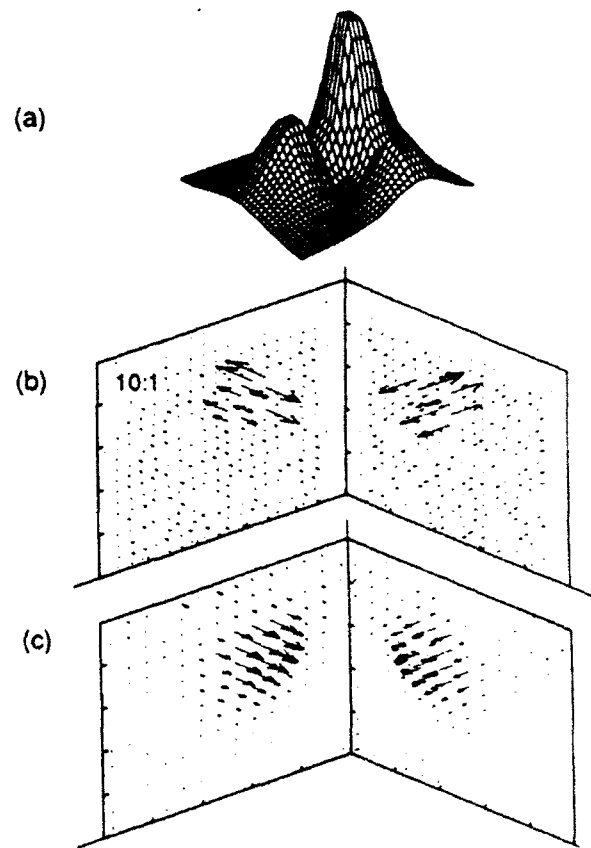

Fig. 7. Similar to Fig. 6, except that two 0.6 cm radius regions, one on each wall of the source surface, have current dipole moments incremented by an average factor of 10. The average power distribution is computed for 100 random arrays of dipole moments. The bottom of the figure shows the current power image distribution determined from the average field power pattern and the known shape of the source surface.
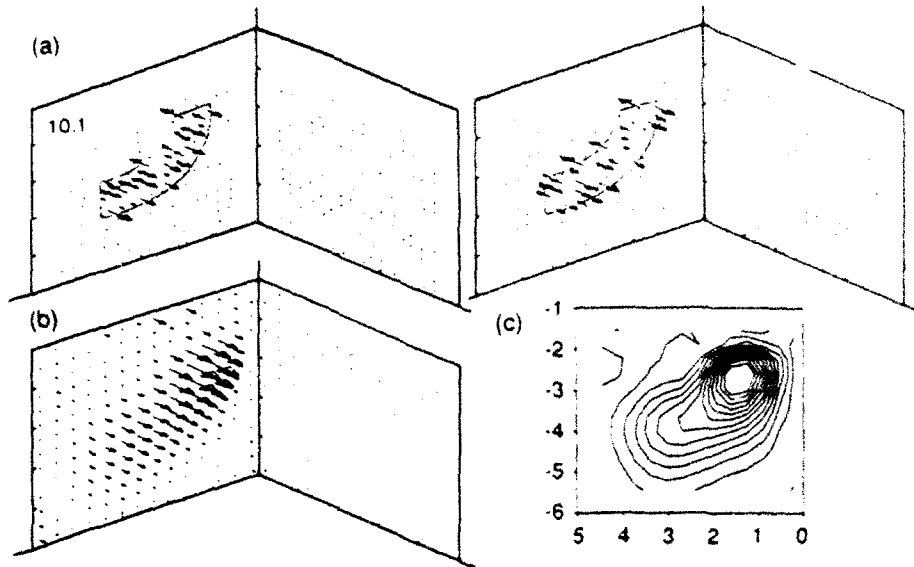
Fig. 8. a: 2 of the 100 samples used in computing average field power for a crescent-shaped area of incoherent activity. (b) The inverse solution representing the spatial distribution of current power and (c) corresponding isodensity current power plot.

tion of field power at the observation plane. Fig. 7c is the inverse solution computed using the extended MNLS.

To illustrate the potential power of this method in delineating the shape of a region of differential incoherent activity, a crescent-shaped portion of the source surface similar to that of Fig. 3 contains current elements which, on average, are 10 times stronger than those of the surrounding region of the surface. The top of the enhanced region is at $z = -2.5$ cm and the bottom at $z = -4.5$ cm. Fig. 8a shows 2 of the 100 samples of the random distributions used in computing the average field power at the observation plane. As before, each of these samples was created by applying different initial seeds to the random number generator. However, the current power image (Fig. 8b) provides a reasonable rendition of the crescent shape. This is made clearer in Fig. 8c by the isocontours of the current power image.

While the enhanced region in the preceding example was, on average, always 10 times that of its surroundings, we also experimented with different ratios. Thus, the 3 plots in Fig. 9 are current power images in which a circular region 0.6 cm in radius is incremented, but the amplitude enhancement is 5 times (Fig. 9a), 4 times (9b), and 3 times (9c) that of the surroundings. Note, these are all drawn with the same scale, while the 10:1 plot of Fig. 6 is shown with a different scale.

If the circular region is moved downward away from the observation plane by 1.5 cm, the center of the region is now at $z = -4.5$ cm and the magnetic field at the observation plane is greatly weakened. In this case,
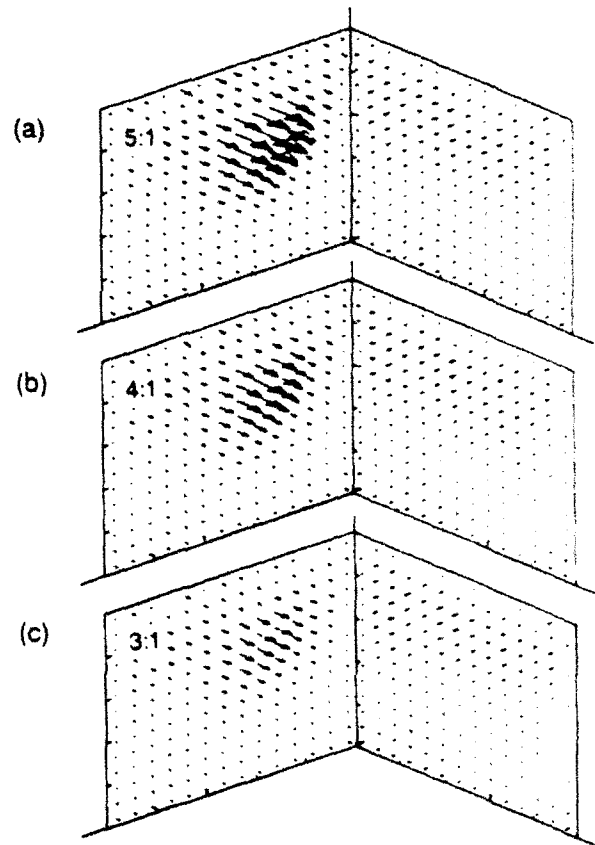

Fig. 9. Image mean power distributions when a region 0.6 cm in radius centered at a depth $z = 3$ cm is incoherently active with dipole moments of current elements incremented by a factor of (a) 5, (b) 4, and (c) 3 times the level of the surroundings. The power levels expressed in the images grow progressively weaker with the reduced ratio.
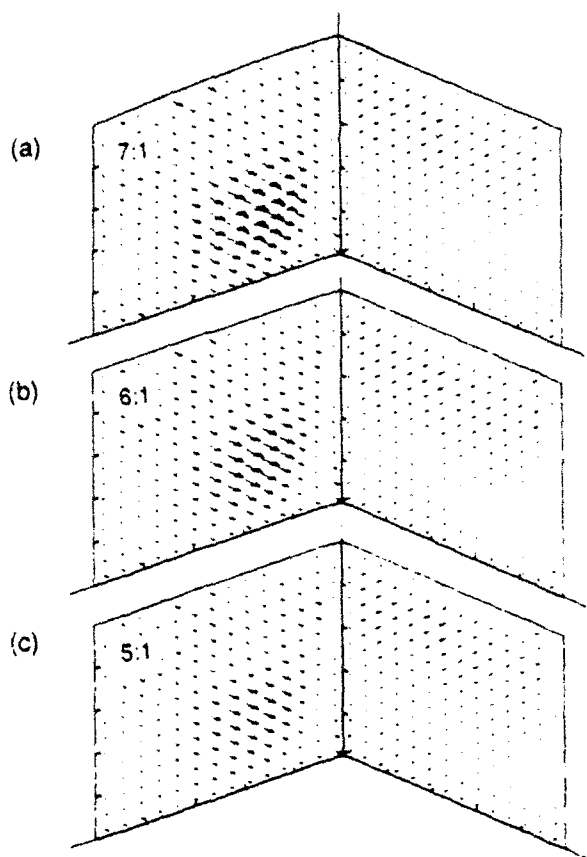
Fig. 10. Similar to Fig. 9, except that the sources are at a depth z = 4.5 cm and dipole moments are incremented by a factor of (a) 7, (b) 6 and (c) 5 times the level of the surroundings.

if the incremented region's strength is less than 5 times that of its surroundings, the incremented region is no longer discriminable in the current power image (Fig. 10). The gradual deterioration in the ability to visualize current power images for incremented regions of a particular size is illustrated in Fig. 10 where the ratios, from top to bottom, are 7:1, 6:1, 5:1, respectively. Note that Figs. 9 and 10 were plotted at the same scale. These examples are meant merely to illustrate the fact that inverse solutions may not be successful for regions with levels of differential activity that are too small considering the distance of the detection coil from the source area, or when the area is smaller than some minimum size. The degree to which these interacting parameters will affect the application of the extended MNLS method in real situations is clearly an empirical question.

Because of these potential problems we devised a variation on the basic method described thus far. This variation significantly enhances the ability to visualize "target" areas in current power images when signal-to-noise ratio, area, and distance were not favorable, as in the foregoing examples. In this variation we first evaluate the field power associated with the overall background when the target area is absent (as shown in

Fig. 4). An example of this in a real situation would be to plot the power of the component of the field normal to the surface of the scalp of a resting human subject. We then find the extended MNLS solution for the current power image to define a *baseline* image of the background. Then the localized area is imposed on this background as, for example, when the subject becomes engaged in a mental task of some kind, thus altering the level of activity of one or more regions of the cortex. We then find the extended MNLS for the current power image with this target area or areas present. Subtracting the image of the baseline distribution from the image containing the target area gives a current power image difference plot, such as those illustrated in Fig. 11. The directions of the arrows in the image surface reflect the sign of the difference between the suppressed and baseline activity. Positive values are indicated by arrows directed toward the reader. Note that the target in Fig. 11a is one that is difficult to visualize in Fig. 10c. Note also that the noise in the surroundings is much improved, even though accentuated by the greater magnification of a factor of 2.5, the scale used to plot the image strength
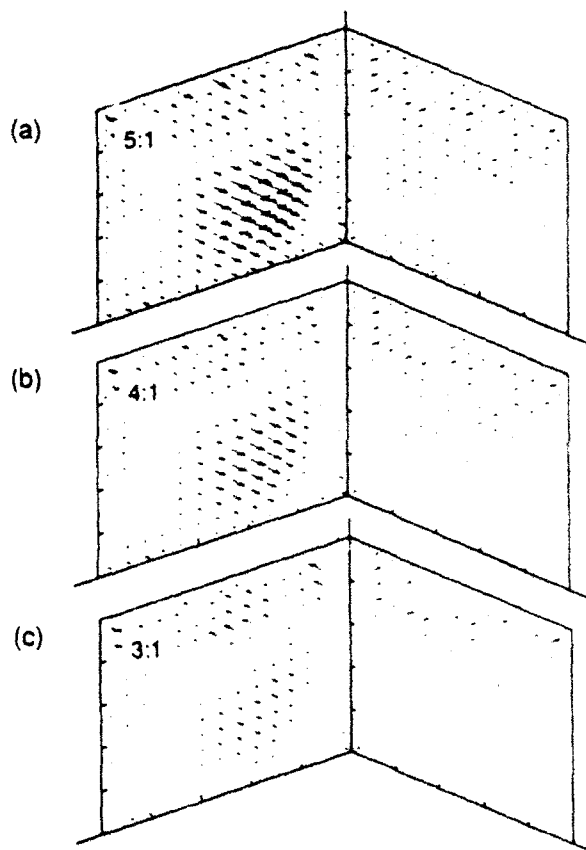

Fig. 11. Image power-difference plots for the sources of Fig. 10, where the image of the background is subtracted from the image of background plus active circular region, for dipole moments in the active region that are incremented by a factor of (a) 5, (b) 4 and (c) 3 times the level of the surroundings.

in Fig. 11. It is very important to emphasize that different initial seeds were been used for simulating the baseline activity and for simulating the activity containing the targets. This indicates that a similar approach may be used in real situations where neuronal activity is simply not going to have a constant distribution over long periods of time, despite the long-term stability of average MEG and EEG power.

Decremented incoherent activity

Thus far we have dealt only with target areas whose activity has a somewhat higher level than that of the surroundings. However, this is a distinction based on an assumed convention. It is equally logical to consider these patterns as those in which the so-called surroundings is decremented as compared to the smaller target areas. So, if very large areas of cortex should exhibit alpha suppression, for example, then the methods we have used would be able to delineate those areas. Moreover, we may also consider the reverse situation, in which the suppressed target region is small relative to the surroundings, since this may have important applications. For example, relatively small cortical regions affected by ischemia may exhibit less overall

Fig. 13. a: crescent-shaped source region of suppressed activity. b: image power distribution difference obtained by subtracting the current power image of 100 samples of (a) from the current power image of 100 samples of uniform activity obtained from different initial seeds. c: image power distribution difference obtained as in (b) but starting from the same initial seeds.
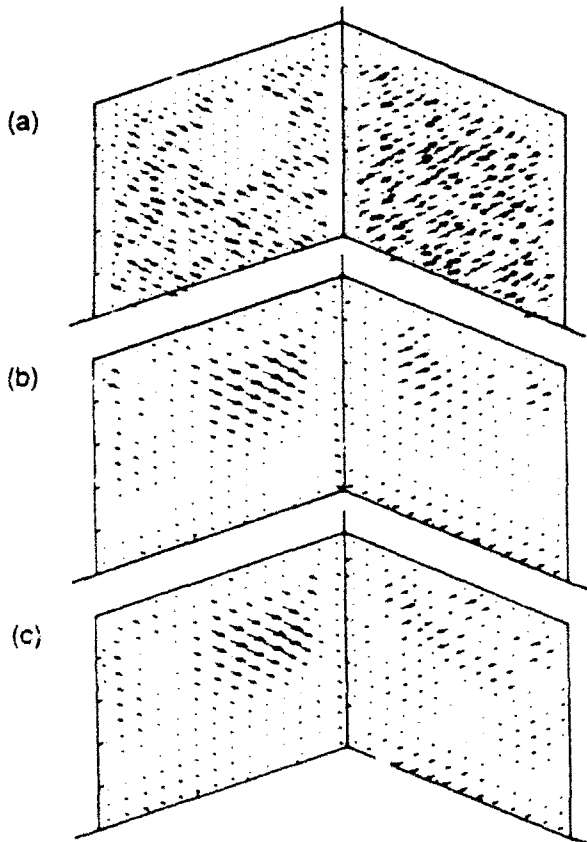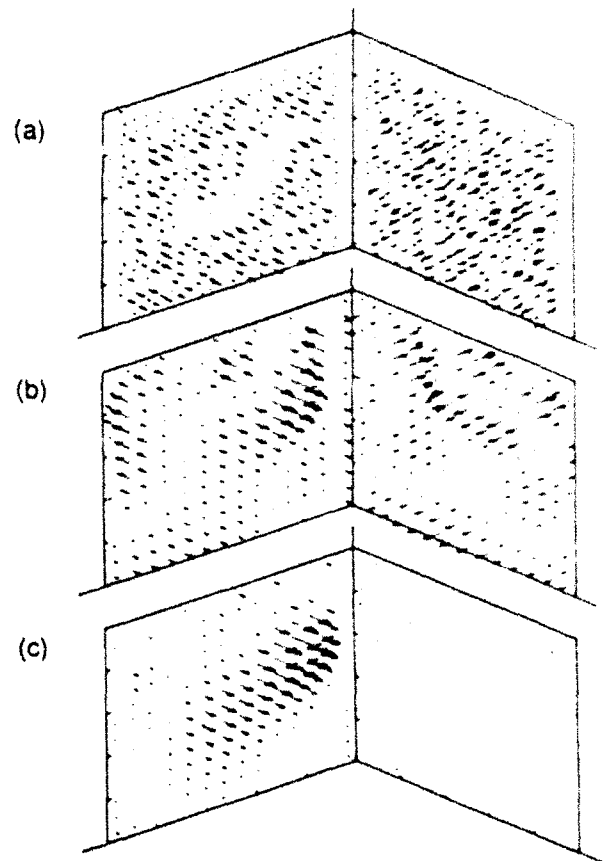

Fig. 12. a: sample of a source distribution with a circular region that is decremented. b, c: image power distributions obtained by subtracting the average of 100 such samples from the baseline inverse of 100 different samples of uniform activity, beginning with different seeds.

activity than their surroundings. Also, as implied in the work of Kaufman et al. (1991b), relatively circumscribed areas may exhibit suppression as subjects engage in scanning short-term memory for tonal stimuli. It would be of considerable value to locate and delineate such areas.

One of the difficulties associated with detecting small decremented target areas is that the extracranial field is dominated by the background activity which originates in a relatively much larger area of cortex. This could result in an extremely disadvantageous signal-to-noise ratio which may make it difficult to detect any change simply by examining at the inverse plots of current power image. While in actual suppression data studied by Kaufman et al. (1990, 1991a) the empirically observed suppression is very pronounced and may often be seen in single trials, this problem could arise in the case of subtler effects. To deal with this in our simulation, we begin with a circular target area having a radius of 1 cm. On average, the strength of activity within this target is 1:10 that of its surroundings. A single sample of a source distribution is shown in Fig.

12a. In our computations, 100 such samples with different initial seeds were used in the simulation. The current power image when the source was decremented was subtracted from the current power image of the baseline. Fig. 12b and c show these power image difference plots. Note again that different initial seeds were used for producing the inverse power with a decremented region and the baseline inverse. This produces patches of activity in the image that differ from one computation to another.

The above procedures were employed to detect a crescent shaped region of suppressed activity (Fig. 13a) with the extended MNLS inverse. Under the conditions of this simulation, where the target pattern extends over a wide range in depth (with the top at $z = -2.5$ cm and the bottom at $z = -4.5$ cm) the lower part of the current power image is buried in the noise (Fig. 13b). Of course, where the surrounding activity is more stable over time, it is possible to obtain an image of higher quality. For example, the plot in Fig. 13c is one where the baseline of uniform activity and the distributions containing the target shapes were created by applying the same initial seed to the random number generator. The resulting power image difference plot shows a well-defined crescent, because there is an "exact" cancellation of the background activity. The poorer image of Fig. 13b results from no correlation of baseline and target, while the higher quality image results from perfect correlation. Empirically, the result will probably be intermediate between these two solutions. In particular, the length of time over which recording are made will have a substantial influence on the quality of the subtraction technique.

Conclusions

The main conclusion of this paper is that it is possible in principle to estimate mathematically unique inverse solutions to recover the location, shape and magnitude of a differentially active region of cortex, even when the activity is incoherent. This, together with earlier work, makes it possible to uniquely define both coherent and incoherent activity using maps of the extracranial field and its power together with MRI-based reconstructions of the individual subject's or patient's brain.

Many problems remain to be overcome before the ideas developed here can be employed in practice. For example, the effects of measurement errors and in accuracy of information about underlying cortical geometry have yet to be fully ascertained. Our own ongoing work suggests that an accuracy of better than 4 mm in knowledge of cortical geometry may be required (Wang 1992; Wang et al. 1992). This is possible with the relatively recent advent of low-distortion 1 mm

resolution MRI systems. However, as a practical matter it is not yet possible to automatically segment cortex from MRI scans and use these regions of interest in constructing accurate 3-dimensional representations of the cortex. Manual methods are widely used, and these are inherently innaccurate. Work towards resolving these problems is underway in our and many other laboratories. Further, effects of noise must also be considered in more detail. Our work (Wang 1992; Wang et al. 1992) shows that the effects of increased noise may be offset by increasing the numbers of positions at which measurements are made, but this too must be investigated further. Extracortical sources of noise require special consideration. At the present time, instrument noise is largely negligible, as modern thin-film SQUID sensors provide noise levels as good as 5 fT$\sqrt{Hz}$, which is a factor of 4 better than older more widely used neuromagnetometer systems. In dealing with intrinsic activity, the fields of interest may range upwards of 1 pT, which is much larger than this instrument noise level. Biological noise sources, e.g., heart and eye movements, are entirely negligible with second-order gradiometers with a 4–5 cm baseline (Romani et al. 1982), but can be consequential when using long baseline first-order gradiometers. Heart signals are unlikely to be sensed by planar gradiometers, for example Hämäläinen 1989). Therefore, interference from extracortical sources is a technical problem that can be dealt with by using an appropriate pickup coil design or by use of adaptive filtering techniques. Changes in the position of cortex time-locked to pulsatile changes in blood volume in the brain are not likely to be of such a magnitude as to be of importance.

Of greater importance is the fact that the adjacent walls of the brain's sulci are often in close proximity to each other, so that it may not be possible to accurately determine the wall to which some change in level of ongoing activity actually belongs. Simulation studies in which actual cortical contours are used may clarify the degree to which this is a problem, and also the degree to which various image enhancement techniques may be employed to sharpen the resolution and how changes in the density of sampling the extracranial magnetic field can affect it. Analogues to the strategies employed in image processing are worthy of further exploration.

Assuming that the differential levels of activity of the different regions of the brain are significantly related to sensory-perceptual and cognitive processes, and all the evidence accumulated thus far suggests that they are, then approach described in this paper makes it possible to envision a new kind of brain mapping. We propose to dub this mapping *dynamic functional imaging* because it will reveal changes in activity in different regions with a temporal resolution measured in fractions of a second. LK put milliseconds here, but

alpha does not change much in 1 ms. PET blood flow methods also provide functional images, but the time resolution is no better than about 40 s, and data must be averaged over subjects. MRI techniques show promise of better temporal resolution, but this possibility remains to be demonstrated.

While we have restricted our discussion to the brain's magnetic field, it may well become possible to develop similar methods in which electroencephalographic data are used instead. In principle there is no reason why this cannot be accomplished, provided that an accurate picture of the electrical properties, e.g., conductivities, of the individual patient's skull, brain, and other tissues that affect the flow of volume currents are taken into account when computing the solution for the inverse problem.

Finally, although we have emphasized the human cerebral cortex throughout, it should be borne in mind that there is no reason why other subcortical nuclei with electrically active laminar structures cannot be treated in the same manner. Here the only real limitations may be the quality of signal-to-noise, as this will be degraded for very deep source surfaces.

It is obvious that the next step will be to implement the extended MNLS procedures using actual subjects and images of their brains. Also, clinical trials should be attempted where there are confirmed abnormal metabolic levels for comparison with PET procedures, and where there is abnormal field power in some bandwidths associated with epileptoid phenomena.

References

Barnett, S. Matrices, Methods and Applications. Clarendon Press, Oxford, 1990.

Ben-Israel, A. and Greville, T.N.E. Generalized Inverses Theory and Applications. Wiley, New York, 1974.

Ciarlet, P.G. Introduction to Numerical Linera Algebra and Optimisation. Cambridge Univ. Press, Cambridge, 1991.

Clarke, C.J.S., Ioannides, A. A. and Bolton, J.P.R. Localised and distributed source solutions for the biomagnetic inverse problem I. In: S.J. Williamson, M. Hoke, G. Stroink and M. Kotani (Eds.), Advances in Biomagnetism. Plenum, New York, 1989: 587-590.

Crowley, C.W., Greenblatt, R.E. and Khalil, I. Minimum norm estimation of current distributions in realistic geometries. In: S.J. Williamson, M. Hoke, G. Stroink and M. Kotani (Eds.), Advances in Biomagnetism. Plenum, New York, 1989: 607-610.

Cuffin, B.N. and Cohen, D. Magnetic fields of a dipole in special volume conductor shapes. IEEE Trans. Biomed. Eng., 1977, BME-24: 372-381.

Cycowicz, Y., Kaufman, L., Williamson, S.J. and Glanzer, M. Differences in brain activity during imaging and verbal tasks. 1992: in preparation.

Dallas, W.J., Fourier space solution to the magnetostatic imaging problem. Appl. Optics, 1985, 24: 4543-4546.

George, J.S., Lewis, P.S., Ranken, D.M., Kaplan, L. and Wood, C.C. Anatomical constraints for neuromagnetic source models. 8th Int. Conf. Biomagn. Abst., 1991: 83.

Graumann, R. The reconstruction of current densities. biomagnetic localization and 3D modeling. In: J. Nenonen, H.-M. Rajala and T. Katila (Eds.), Report TKK-F-A689. Helsinki University of Technology, Otaniemi, 1991: 172-186.

Greenblatt, R.E. Spatiotempral likelihood estimator solutions to the bioelectromagnetic inverse problem. 8th Int. Conf. Biomagn. Abst., 1991: 329.

Hämäläinen, M.S. A 24-channel planar gradiometer system design and analysis of neuromagnetic data. In: S.J. Williamson, M. Hoke, G. Stroink and M. Kotani (Eds.), Advances in Biomagnetism. Plenum, New York, 1989: 639-644.

Hämäläinen, M.S. and Ilmoniemi, R.J. Interpreting Measured Magnetic Fields of The Brain: Estimates of Current Distributions. Report TKK-F-A559. Helsinki University of Technology, Otaniemi, 1984.

Hämäläinen, M.S. and Ilmoniemi, R.J. Interpreting magnetic fields of the brain: minimum-norm estimates. IEEE Trans. Biomed. Eng., 1992: in press.

Ioannides, A.A., Bolton, J.P.R., Hasson, R. and Clarke, C.J.S. Localised and distributed source solutions for the biomagnetic inverse problem II. In: S.J. Williamson, M. Hoke, G. Stroink and M. Kotani (Eds.), Advances in Biomagnetism. Plenum, New York, 1989: 591-594.

Ioannides, A.A., Bolton, J.P.R. and Clarke, C.J.S. Continuous probabilistic solutions to the biomagnetic inverse problem. Inverse Problems, 1990, 6: 1-20.

Kaufman, L., Schwartz, B., Salustri, C. and Williamson, S.J. Modulation of spontaneous brain activity during mental imagery. Cogn. Neurosci., 1990, 2: 124-132.

Kaufman, L., Kaufman, J.H. and Wang, J.-Z. On cortical folds and neuromagnetic fields. Electroenceph. clin. Neurophysiol., 1991, 79: 211-226.

Kaufman, L., Curtis, S., Wang, J.-Z. and Williamson, S.J. Changes in cortical activity when subjects scan memory for tones. Electroenceph. clin. Neurophysiol., 1992, 82: 266-284.

Kullmann, W.H. Can volume conductor modeling improve biomagnetic distributed source imaging? Biomagnetic localization and 3D modeling. In: J. Nenonen, H.-M. Rajala and T. Katila (Eds.), Report TKK-F-A689. Helsinki Univ. of Technology, Otaniemi, 1991: 137-153.

Kullmann, W.H. and Dallas, W.J. Fourier imaging of electrical currents in the human brain from their magnetic fields. IEEE Trans. Biomed. Eng., 1987, BME-34: 837-842.

Kullmann, W.H., Jandt, K.D., Rehm, K., Schlitt, H.A., Dallas, W.J. and Smith, W.E. A linear estimation approach to biomagnetic imaging. In: S.J. Williamson, M. Hoke, G. Stroink and M. Kotani (Eds.), Advances in Biomagnetism. Plenum, New York, 1989: 571-574.

Mosher, J.C., Lewis, P.S. and Leahy, R.M. Multiple dipole modelling and localization from spatio-temporal MEG data. IEEE Trans. Biomed. Eng., 1992, 39: 541-557.

Okada, Y.C. and Huang, J.C. Current-density imaging as method of visualizing neuronal activities of the brain. Soc. Neurosci. Abst., 1990, 16: 1241.

Okada, Y.C., Huang, J.C. and Xu, C. A hierarchical minimum norm estimation method for reconstructing current densities in the brain from remotely measured magnetic fields. 8th Int. Conf. Biomagn. Abst., 1991: 152.

Penrose, R. A generalized inverse for matrices. Proc. Cambridge Phil. Soc., 1955, 51: 406-413.

Pfurtscheller, G. Mapping of event-related desynchronization and type of derivation. Electroenceph. clin. Neurophysiol., 1988, 70: 190-193.

Pfurtscheller, G. and Aranibar, A. Event-related cortical desynchronization detected by power measurements of scalp EEG. Electroenceph. clin. Neurophysiol., 1977, 42: 817-826.

Pfurtscheller, G., Steffan, J. and Maresch, H. ERD-mapping and functional topography - temporal and spatial aspects. In: G.

Pfurtschuller and F.H. Lopes da Silva (Eds.), Functional Brain Imaging. Huber, Toronto, 1988: 117–130.

Plonsey, R. Capability and limitations of electrocardiography and magnetocardiography. IEEE Trans. Biomed. Eng., 1972, BME-19: 239.

Press, W.H., Flannery, B.P., Teukolsky, S.A. and Vetterling, W.T. Numerical Recipes, the Art of Scientific Computing. Cambridge Univ. Press, Cambridge, 1986.

Regan, D.M. Human Brain Electrophysiology: Evoked Potentials and Evoked Magnetic Fields in Science and Medicine. Elsevier Science Publishers, Amsterdam, 1989.

Robinson, E.S. Current source image estimation by spatially filtered MEG. 8th Int. Conf. Biomagn. Abst., 1991: 337.

Romani, J.-L., Williamson, S.J. and Kaufman, L. Biomagnetic instrumentation. Rev. Sci. Instrum., 1982, 53: 1815–1845.

Roth, B.J., Sepulveda, N.G. and Wikswo, Jr., J.P. Using a magnetometer to image a two-dimensional current distribution. J. Appl. Phys., 1989, 65: 361–372.

Scherg, M. Fundamentals of dipole source analysis. In: F. Grandori, M. Hoke and G.L. Romani (Eds.), Advances in Audiology: Auditory Evoked Magnetic Fields and Electric Potentials. Karger, Munich, 1990: 40–69.

Scherg, M. and Von Cramon, D. Two bilateral sources of the AEP as identified by a spatio-temporal dipole model. Electroenceph. clin. Neurophysiol., 1985, 62: 32–44.

Singh, M., Doria, D., Henderson, V.W., Huth, G.C. and Beatty, J.

Reconstruction of images from neuromagnetic fields. IEEE Trans. Nucl. Sci., 1984, NS-31: 585–589.

Sternberg, S. High speed scanning in human memory. Science, 1966, 153: 652–654.

Szinger, J. and Kuc, R. Application of the SVD to biomagnetic imaging. 8th Int. Conf. Biomagn. Abst., 1991: 421.

Tan, S., Roth, B.J. and Wikswo, Jr., J.P. The magnetic field of cortical current sources: the application of a spatial filtering model to the forward and inverse problems. Electroenceph. clin. Neurophysiol., 1990, 76: 73–85.

Wang, J.-Z. "Minimum-norm least-squares estimation, unique magnetic source images for a spherical model head". 1992: submitted for publication.

Wang, J.-Z., Williamson, S.J. and Kaufman, L. Magnetic source images determined by a lead-field analysis: the unique minimum-norm least-squares estimation. IEEE Trans. Biomed. Eng., 1992, BME-39: 665–675.

Williamson, S.J. and Kaufman, L. Magnetic fields of the cerebral cortex. In: S.N. Erné, H.D. Hahlbohm and H. Lübbig (Eds.), Biomagnetism. Walter de Gruyter, Berlin, 1981: 353–401.

Williamson, S.J. and Kaufman, L. Analysis of neuromagnetic signals. In: A.S. Gevins and A. Rémond (Eds.), Handbook of Electroenceph. clin. Neurophysiol., Vol. 1. Methods of Analysis of Brain Electrical and Magnetic Signals. Elsevier, Amsterdam, 1987: 405–444.